Appl Nanosci (2016) 6:301–307
DOI 10.1007/s13204-015-0440-8

ORIGINAL ARTICLE

Fabrication of quantum dot/silica core–shell particles immobilizing Au nanoparticles and their dual imaging functions

Yoshio Kobayashi[1] · Hiromu Matsudo[1] · Ting-ting Li[1] · Kyosuke Shibuya[1] · Yohsuke Kubota[2] · Takahiro Oikawa[2] · Tomohiko Nakagawa[2] · Kohsuke Gonda[2]

Received: 4 December 2014 / Accepted: 17 March 2015 / Published online: 31 March 2015

Abstract The present work proposes preparation methods for quantum dot/silica (QD/SiO_2) core–shell particles that immobilize Au nanoparticles (QD/SiO_2/Au). A colloid solution of QD/SiO_2 core–shell particles with an average size of 47.0 ± 6.1 nm was prepared by a sol–gel reaction of tetraethyl orthosilicate in the presence of the QDs with an average size of 10.3 ± 2.1 nm. A colloid solution of Au nanoparticles with an average size of 17.9 ± 1.3 nm was prepared by reducing Au^{3+} ions with sodium citrate in water at 80 °C. Introduction of amino groups to QD/SiO_2 particle surfaces was performed using (3-aminopropyl)-triethoxysilane (QD/SiO_2-NH_2). The QD/SiO_2/Au particles were fabricated by mixing the Au particle colloid solution and the QD/SiO_2-NH_2 particle colloid solution. Values of radiant efficiency and computed tomography for the QD/SiO_2/Au particle colloid solution were 2.23×10^7 (p/s/cm^2/sr)/(μW/cm^2) at a QD concentration of 8×10^{-7} M and 1180 ± 314 Hounsfield units and an Au concentration of 5.4×10^{-2} M. The QD/SiO_2/Au particle colloid solution was injected into a mouse chest wall. Fluorescence emitted from the colloid solution could be detected on the skin covering the chest wall. The colloid solution could also be X-ray-imaged in the chest wall. Consequently, the QD/SiO_2/Au particle colloid solution was found to have dual functions, i.e., fluorescence emission and X-ray absorption in vivo, which makes the colloid solution suitable to function as a contrast agent for dual imaging processes.

Keywords Quantum dot · Au · Nanoparticle · Silica coating · Core–shell · Fluorescence imaging · X-ray imaging

Introduction

Nanoparticles of semiconductor compounds such as CdS, CdSe, and CdTe exhibit unique fluorescent properties and are called quantum dots (QDs). QDs have often been used as a contrast agent for in vivo fluorescence imaging (Ozawa et al. 2013; Sapsford et al. 2013; Geißler et al. 2014).

Because these QDs contain cadmium, they might harm living tissues (Yang et al. 2012; Tassali et al. 2014; Bereza-Malcolm et al. 2015). Coating the QDs with materials inert to living organisms forms core–shell particles with a QD core; the inert shell prevents contact with living tissues because of the physical barrier of the shell. Accordingly, forming such core–shell structures is a candidate method for reducing toxicity. Shell materials should be chemically inert in a wide variety of solvents and nontoxic to living organisms. Core–shell particles with QD nanoparticle cores must flow without aggregating in the blood vessels of an organism after injection because blood flow is weakened or stopped by such aggregation.

Silica is chemically inert and nontoxic relative to many solid materials (Hu et al. 2013; Young and Santra 2014; Zeng et al. 2014). Because silica particles form stable colloids in various dispersions (Mondragon et al. 2012; Bitter et al. 2013; Chou et al. 2014), silica-coated particles

✉ Yoshio Kobayashi
ykoba@mx.ibaraki.ac.jp

[1] Department of Biomolecular Functional Engineering, College of Engineering, Ibaraki University, 4-12-1 Naka-narusawa-cho, Hitachi, Ibaraki 316-8511, Japan

[2] Department of Medical Physics, Graduate School of Medicine, Tohoku University, Sendai, Miyagi 980-8575, Japan

become highly dispersed, which provides steady particle flow in blood vessels. Accordingly, silica is a promising shell material. Silica particles can be easily fabricated via the Stöber method (Bell et al. 2012; Goertz et al. 2012; Neville et al. 2012; Börner et al. 2013). Several researchers have extended the Stöber method to produce QDs coated with silica, or QD/SiO_2 core–shell particles (Wang et al. 2012; Ma et al. 2014; Aubert et al. 2014). Their method uses a sol–gel reaction with silicone alkoxide and base catalyst in the presence of the QDs. Our research group has proposed an alternative method for producing QD/SiO_2 particles (Kobayashi et al. 2010a, b, 2012a, 2013a, 2015) and performed fluorescence imaging of mice tissues, into which the colloid nanoparticle solutions were injected (Kobayashi et al. 2013a, 2015).

Materials with high X-ray absorption properties can be applied for X-ray imaging techniques. In imaging, iodinated contrast agents are usually used to obtain clear images. Typical X-ray contrast agents that are commercially available are iodine compounds dissolved homogeneously in solvents at the molecular level. However, iodine compound X-ray contrast agents face a problem; they may provoke adverse events such as allergic reactions in patients (Lusic and Grinstaff 2013; Scoditti et al. 2013; Wendel et al. 2014), preventing their administration to such people. In addition to iodine compounds, Au is also promising for imaging because Au also highly absorbs X-rays and is less toxic relative to the iodine compounds. From this viewpoint, Au nanoparticles have been examined with respect to their use as contrast agents for imaging tissues in living bodies at the nanometer level (Lusic and Grinstaff 2013; Cole et al. 2014; Betzer et al. 2014).

Materials composed of components that have different properties should have multiple functions. Considering the multi-functionalization of materials, particles containing QDs and Au will act as both a fluorescent contrast agent and an X-ray contrast agent. The present work proposes a method for fabricating composite particles composed of QD/SiO_2 core–shell particles and Au nanoparticles, or QD/SiO_2 core–shell particles on which Au nanoparticles are immobilized (QD/SiO_2/Au). QD/SiO_2 core–shell particles were fabricated according to the method outlined in our previous works (Kobayashi et al. 2010a, b, 2012a, 2013a, 2015), and amino groups were introduced onto their surface using silicone alkoxide with a terminal amino group. Au nanoparticles were prepared with a conventional method using citrate as a reducing reagent. The QD/SiO_2/Au particles were fabricated by simply mixing the QD/SiO_2 core–shell particle colloid solution and the Au nanoparticle colloid solution. Imaging abilities based on both fluorescence and X-ray absorption of the composite particle colloid solution were also studied in the present work.

Experimental

Chemicals

Qdot® (Invitrogen Co., catalog number: Q21371MP, concentration: 8×10^{-6} M), $CdSe_xTe_{1-x}$ nanoparticles coated with ZnS and then surface-modified with carboxyl groups, was the seed QD nanoparticle for the silica coating. Figure 1a shows a transmission electron microscope (TEM) image of these QDs. Their average size was 10.3 ± 2.1 nm. According to our previous work, the QD emits fluorescence with a peak at around 745 nm (Kobayashi et al. 2010b). For silica coating of the QD nanoparticles, the sol–gel silica source, catalyst, and solvent were tetraethyl orthosilicate (TEOS) (Kanto Chemical Co., Inc., 95 %), sodium hydroxide (NaOH) (Kanto Chemical Co., Inc., 0.1 M), and ethanol (Kanto Chemical Co., Inc., 99.5 %), respectively. Au nanoparticles were prepared using hydrogen tetrachloroaurate (III) trihydrate ($HAuCl_4 \cdot 3H_2O$) (Sigma-Aldrich, >98 %) and trisodium citrate dihydrate (Na-cit) (Kanto Chemical, 99 %). (3-aminopropyl)triethoxysilane (APES) (Tokyo Chemical Industry, 98 %) was used for introducing amino groups on the QD/SiO_2 particle surface to increase the affinity between the Au particle surface and the QD/SiO_2 particle surface. All chemicals were used as received. Water that had been ion-exchanged and distilled with a Shimadzu SWAC-500 was used for all the preparations.

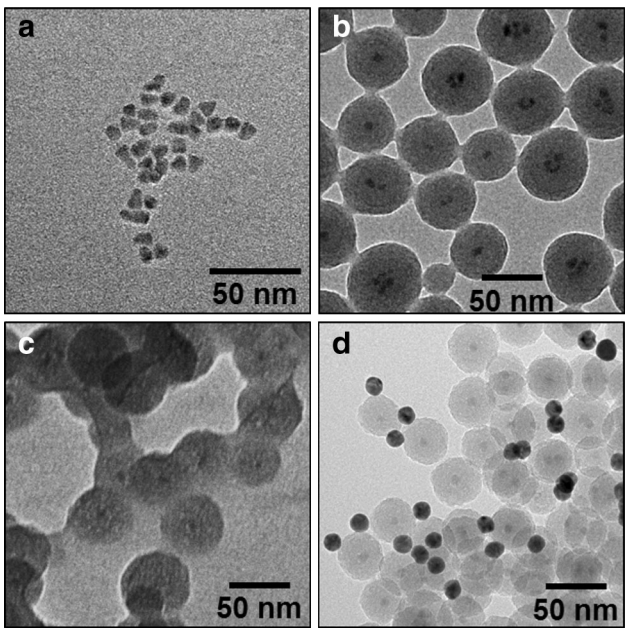

Fig. 1 TEM images of **a** QDs, **b** QD/SiO_2 particles, **c** QD/SiO_2-NH_2 particles, and **d** QD/SiO_2/Au particles

Preparation

The QD nanoparticles were silica-coated via the sol–gel method using TEOS, similarly to the method outlined in our previous works (Kobayashi et al. 2010a, b, 2012a, 2013a, 2015). Solutions of 38.0 mL of 18.4/81.6 (v/v) water/ethanol and 11.8 mL of 4.24×10^{-3} M TEOS/ethanol were added to 0.004 mL of the 8×10^{-6} M QD colloid solution in turn. The sol–gel reaction was then initiated by rapidly injecting 0.2 mL of 0.1 M aqueous NaOH into 49.8 mL of the QD/TEOS colloid solution, which resulted in the (0.1 M aqueous NaOH)/(QD/TEOS colloid solution) volume ratio of 0.402 %. The above-mentioned amounts of solutions gave the initial concentrations of 6.4×10^{-10} M QD, 1.0×10^{-3} M TEOS, 8 M H_2O, and 4.0×10^{-4} M NaOH. The reaction proceeded for 24 h at room temperature. Our previous work indicated no serious effect of the silica coating on emission wavelength and fluorescence intensity of QDs (Kobayashi et al. 2010b). The QD/SiO_2 colloid solution prepared in the present work was also considered to have the same fluorescence properties as the QD colloid solution. The QD/SiO_2 colloid solution was concentrated to a QD concentration of 3.2×10^{-9} M by evaporating the solvent, centrifuging, removing the supernatant, adding water, and redispersing the concentrated QD/SiO_2 colloid solution.

A freshly prepared 0.118 mL of 0.339 M Na-cit aqueous solution was added to 24.9 mL of 2.41×10^{-4} M $HAuCl_4$ aqueous solution at a constant temperature of 80 °C under vigorous stirring, which resulted in initial concentrations of 2.4×10^{-4} M Au and 1.6×10^{-3} M Na-cit.

For efficient immobilization of Au nanoparticles on the QD/SiO_2 particle surface, or production of QD/SiO_2/Au particles, amino groups were first introduced on the QD/SiO_2 particle surface using APES (QD/SiO_2-NH_2), because the alkoxide groups of the APES were expected to react with the OH groups on the silica surface of the QD/SiO_2 particles. APES (0.035 mL) was added to 25 mL of the concentrated QD/SiO_2 colloid solution with the QD concentration of 3.2×10^{-9} M at room temperature, which resulted in an initial APES concentration of 6×10^{-3} M. In a preliminary experiment, an iso-electric point of the QD/SiO_2-NH_2 particles shifted to high pH with the introduction of amino groups, and the shift was the largest at the initial APES concentration of 6×10^{-3} M in an initial APES concentration range of 6×10^{-5} to 6×10^{-2} M, which indicated that efficient introduction of amino groups was performed at 6×10^{-3} M. Thus, the initial APES concentration was adjusted to 6×10^{-3} M in the present work. The reaction time was 24 h. The QD/SiO_2-NH_2 colloid solution was concentrated to a QD concentration of 1.28×10^{-7} M by centrifuging, removing the supernatant, adding ethanol, and redispersing the concentrated QD/SiO_2-NH_2 colloid solution. For the Au nanoparticles' immobilization, ethanol, water, and the Au nanoparticle colloid solution were added in turn to the QD/SiO_2-NH_2 particle colloid solution at 35 °C, as the amino groups on the particle surface were expected to coordinate with the surface of Au nanoparticles. The initial concentrations of QD, Au, and H_2O were 7.4×10^{-10}, 5×10^{-5}, and 12.4 M, respectively. The QD/SiO_2/Au colloid solution was concentrated by evaporating the solvent, centrifuging, removing the supernatant, adding water, and redispersing the colloid solution, which produced a QD/SiO_2/Au colloid solution with a QD concentration of 8.0×10^{-7} M and an Au concentration of 5.4×10^{-2} M

Characterization

The samples were characterized by ultra-visible (UV–VIS) spectroscopy, electrophoretic light scattering (ELS), and TEM. VIS extinction of the particle colloid solution was measured with a Shimadzu UV-3101PC (Kyoto, Japan) spectrophotometer. ζ-potentials of the particles were measured by ELS to obtain information on the state of the particles. The ELS was performed with a Malvern Zetasizer Nano ZS90 (Worcestershire, UK). Either an HCl aqueous solution or an NaOH aqueous solution was added to the solution to vary the pH of the solution for the ELS measurement. The TEM imaging was performed using a JEOL JEM-2100 microscope operating at 200 kV. The TEM samples were prepared by dropping the nanoparticle suspensions onto a collodion-coated copper grid and evaporating them. Tens of particle diameters were measured using the TEM images to determine the volume-averaged particle size and its standard deviation.

Fluorescence imaging and X-ray imaging with the particle colloid solutions were performed using a Xenogen IVIS 100 fluorometer in vivo imaging system (IVIS) and an Aloka La theta LCT-200 CT system, Japan), respectively, which were also used in our previous works (Ayame et al. 2011; Kobayashi et al. 2011, 2012b, 2013a, b, c, d, 2014, 2015). CT values were estimated on the basis of CT values of −1000 and 0 for air and water, respectively. For mouse imaging, the colloid solution (50 μL) was injected into the chest wall of an anesthetized mouse. Fluorescence emitted from inside the colloid-injected mouse was detected with the IVIS. X-ray images of the colloid-injected mouse were taken by transmitting X-rays through the mouse with the CT system. The mice used were ICR mice, aged 5–6 weeks.

Results and discussion

Particle morphology

Figure 1b shows a TEM micrograph of the QD/SiO_2 nanoparticles. The darker and lighter sections of the particles were determined to be the QD particles and silica, respectively, because of their differing electron densities. Most of the particles contained a few QD cores, and the average particle size was 47.0 ± 6.1 nm. Figure 2a shows the ζ-potential of the QD/SiO_2 particles as a function of pH. The ζ-potential decreased and passed through an isoelectric point (IEP) of 3.1 as the pH increased. According to studies performed by several researchers (Kim et al. 2009; Jiang et al. 2012; Zhang et al. 2013), silica particles produced by a sol–gel method using silicon alkoxide have an IEP of 2.0–4.0. The IEP of QD/SiO_2 particles was similar to the IEP for silica particles. This implied that the QD surface was covered with silica, which was supported by the TEM observations (Fig. 1b).

The QD/SiO_2-NH_2 nanoparticles dispersed well in water, or they were colloidally stable, which indicated no serious effect of the APES addition on their colloidal stability in water. Figure 1c shows a TEM micrograph of the QD/SiO_2-NH_2 nanoparticles. Some particles appeared to form aggregates composed of several particles that were likely to precipitate. However, no precipitates were found in the particle colloid solution. Accordingly, the aggregates were thought to be produced during the preparation of TEM samples accompanied by the evaporation of solvent on the TEM grid. Similarly to the QD/SiO_2 nanoparticles, particles containing a few QD cores were observed. Their average particle size was 42.4 ± 4.3 nm, which was considered to be almost the same as that of the QD/SiO_2 nanoparticles within the statistical error. This similarity indicated that their core–shell structure was chemically stable, even after the amination process. Figure 2b shows the ζ-potential of the QD/SiO_2-NH_2 particles as a function of pH. Similarly to the case of QD/SiO_2 nanoparticles, the ζ-potential decreased and passed through an IEP with an increase in pH. The IEP was 9.5, which was higher than that of the QD/SiO_2 nanoparticles. This higher IEP was within a range of 9–11, which is typical of acid dissociation constants for amino groups in many types of amines, such as ammonia, alkylamine, and dialkylamine. Accordingly, this result confirmed that the amino groups were successfully introduced onto the particle surface.

One of the insets in Fig. 3 shows a photograph of the Au nanoparticle colloid solution. After the addition of the Na-cit solution to the $HAuCl_4$ solution, the color of the solution turned wine-red within a few minutes, which implied the formation of Au nanoparticles. Figure 3 shows the extinction spectrum of the Au nanoparticle colloid solution. A peak observed at 521 nm could be attributed to the surface plasmon resonance of Au nanoparticles (Lismont and Dreesen 2012; Liang et al. 2012; Ujihara and Imae 2013). This measurement confirmed that Au nanoparticles were produced, which supports the implication of Au nanoparticle formation. A TEM image of the Au nanoparticles is shown in another inset in Fig. 3. Spherical Au nanoparticles with an average size of 17.9 ± 1.3 nm were observed.

Figure 1d shows a TEM micrograph of the QD/SiO_2/Au nanoparticles. All the Au nanoparticles were immobilized on the particle surface, indicating that the Au nanoparticles' immobilization was successfully performed with the present method. Several Au nanoparticles-free particles were also observed, since a number-ratio of Au nanoparticles/QD/SiO_2-NH_2 nanoparticles was small compared to 1/1. Accordingly, optimization of fabrication conditions such as concentrations of Au nanoparticles and QD/SiO_2-NH_2 nanoparticles in the final colloid solution, reaction

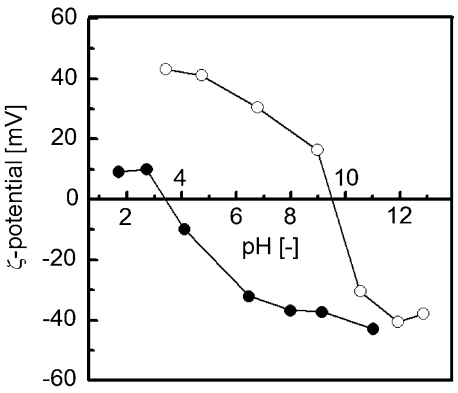

Fig. 2 ζ-potentials of (*filled circle*) QD/SiO_2 particles and (*unfilled circle*) QD/SiO_2-NH_2 particles as a function of pH

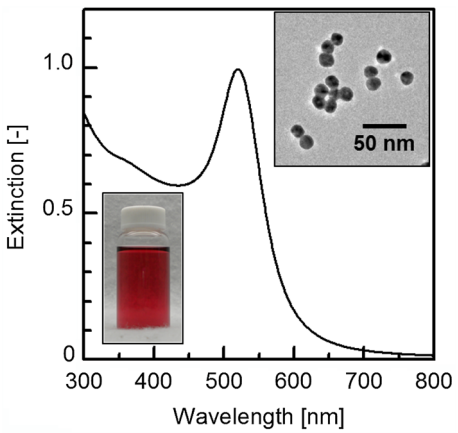

Fig. 3 Extinction spectrum of a colloid solution of Au nanoparticles. *Insets* show a photograph of the colloid solution and a TEM image of the particles

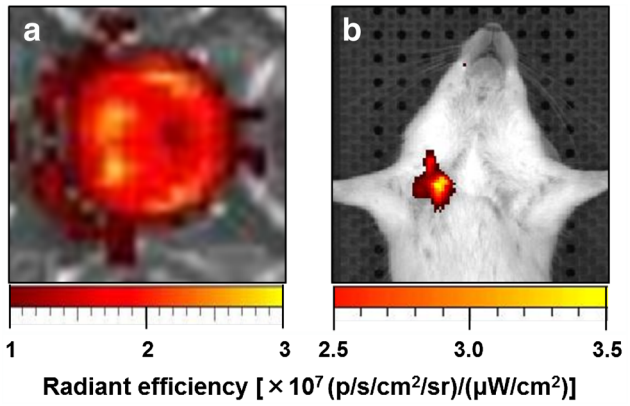

Fig. 4 IVIS images of **a** the QD/SiO_2/Au particle colloid solution and **b** a mouse after the colloid solution was injected into its chest wall

temperature and stirring rate is required to improve the efficiency of Au nanoparticles' immobilization. This improvement may also improve dual imaging ability of the QD/SiO_2/Au particle colloid solution.

Imaging of the QD/SiO_2/Au particle colloid solution

Figure 4a shows an IVIS image of the QD/SiO_2/Au particle colloid solution. The colloid solution was successfully imaged. Its radiant efficiency (RE) was 2.23×10^7 (p/s/cm^2/sr)/(μW/cm^2). The value was converted into a value with respect to QD concentration to compare it with that of a commercial QD. Because the colloid solution had a QD concentration of 8×10^{-7} M, the converted RE was 2.79×10^{13} (p/s/cm^2/sr)/(μW/cm^2)/M. According to our previous work (Kobayashi et al. 2013a), the RE of QDs was 2.93×10^9 (p/s/cm^2/sr)/(μW/cm^2) at a QD concentration of 1×10^{-7} M, which corresponded to a converted RE of 2.93×10^{16} (p/s/cm^2/sr)/(μW/cm^2)/M. The converted RE for the QD/SiO_2/Au particle colloid solution was smaller than that for a commercial QD. The Au nanoparticle colloid solution absorbed visible light in a wide range around the wavelength of 521 nm, as shown in Fig. 3. The fluorescence from the QD/SiO_2/Au particles was probably diminished by this absorption, though the mechanism is still unclear. Although the converted RE for the QD/SiO_2/Au particle colloid solution was small, the intensity of the RE was high enough to image a mouse, based on our previous experience in animal experiments.

Figure 5b shows an X-ray image of the QD/SiO_2/Au particle colloid solution. For comparison, an X-ray image of water is shown in Fig. 5a. The white contrast in the image of the QD/SiO_2/Au particle colloid solution was lighter than that for water. The computed tomography (CT) value of the QD/SiO_2/Au particle colloid solution was 1180 ± 314 Hounsfield units (HU) at an Au concentration of 5.4×10^{-2} M. This value was converted into a value with respect to the molar concentration of subject materials such as Au and I (converted CT value) to compare it with that of a commercial contrast agent. The converted CT value with respect to the Au concentration was estimated to be 2.19×10^4 HU/M. According to our previous work (Kobayashi et al. 2013c), the converted CT value with respect to the iodine concentration for Iopamiron 300 is 4.76×10^3 HU/M. The converted CT value of the QD/SiO_2/Au particle colloid solution was larger than that of Iopamiron 300. Because gold absorbs X-rays more than iodine on the atomic level because of its large atomic number, a larger converted CT value was shown for the QD/SiO_2/Au particle colloid solution. Thus, it was confirmed that the QD/SiO_2/Au particle colloid solution had an ability to function as a highly sensitive X-ray contrast agent.

Mouse imaging

Figure 5c shows an IVIS image of a mouse after the injection of the QD/SiO_2/Au particle colloid solution. Fluorescence was clearly observed on the chest of the mouse after injection into its chest wall, which meant that fluorescence penetrated through the chest skin from inside the mouse to outside. Its radiant efficiency was 3.30×10^7 (p/s/cm^2/sr)/(μW/cm^2). This value was ca. 1.5 times larger than the value of 2.23×10^7 (p/s/cm^2/sr)/(μW/cm^2) for the QD/SiO_2/Au particle colloid solution, which indicated that the QD/SiO_2/Au particle colloid solution could emit strong fluorescence even inside living bodies without quenching.

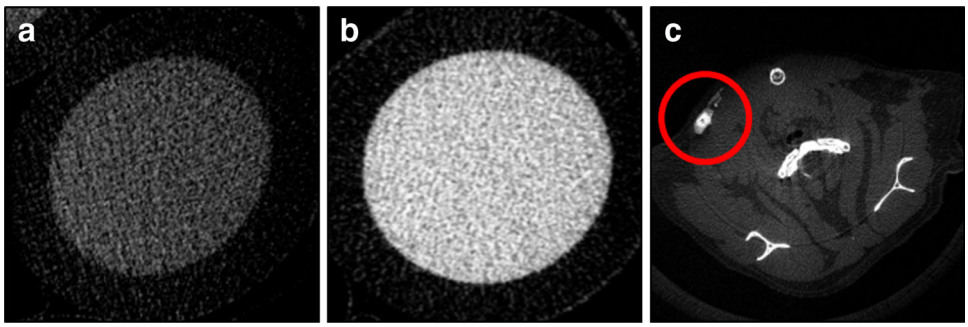

Fig. 5 CT images of **a** water, **b** the QD/SiO_2/Au particle colloid solution, and **c** a mouse after the colloid solution was injected into its chest wall. The QD/SiO_2/Au particle colloid solution was observed in the chest wall, as shown by the *red circle*

The detection of large radiant efficiency implied that the QD/SiO_2/Au particles were accumulated in the chest wall, though the reason for the large radiant efficiency is still unclear.

Figure 5c shows an X-ray image of the mouse after it was injected with the QD/SiO_2/Au particle colloid solution. The location of the particle colloid solution could be recognized clearly at its chest wall because of its light contrast. Its CT value was 1060 ± 374 HU, which was as high as the value of 1180 ± 314 HU for the QD/SiO_2/Au particle colloid solution. Similarly to the fluorescence imaging, it was found that the QD/SiO_2/Au particle colloid solution could be clearly observed even inside living bodies without quenching.

Another result of note is that when the mouse that was injected with the QD/SiO_2/Au particle colloid solution was imaged simultaneously with the IVIS and X-ray, the position imaged by the IVIS was the same as that from X-ray imaging. This result suggests that the colloid solution can function as a contrast agent for dual imaging processes.

Conclusion

QD/SiO_2 particles averaging 47.0 ± 6.1 nm in size were produced via the sol–gel method using TEOS and NaOH in a water/ethanol solution containing QDs. The QD/SiO_2 particles were aminated by reacting silanol groups on the QD/SiO_2 particle surface and alkoxide groups in APES. Au nanoparticles averaging 17.9 ± 1.3 nm in size were produced by reducing $HAuCl_4$ with Na-cit in water. The Au nanoparticles were immobilized on particles via the reaction of amino groups on the QD/SiO_2 particle surface and the Au particle surface. A QD/SiO_2/Au particle colloid solution with a QD concentration of 8×10^{-7} M and an Au concentration of 5.4×10^{-2} M had a radiant efficiency of 2.23×10^7 (p/s/cm^2/sr)/(μW/cm^2) and a CT value of 1180 ± 314 HU. After injection of the QD/SiO_2/Au particle colloid solution into the chest wall of a mouse, the colloid solution could be detected simultaneously with IVIS and CT on the skin covering the chest wall and in the chest wall, respectively. Accordingly, the QD/SiO_2/Au particle colloid solution has the potential to be used as a contrast agent with dual functions for techniques such as fluorescence emission and X-ray absorption in vivo.

Acknowledgments This work was supported by JSPS KAKENHI Grant Number 24310085, and by a Grant-in-Aid for Scientific Research on Innovative Areas "Nanomedicine Molecular Science" (No. 2306) from the Ministry of Education, Culture, Sports, Science, and Technology of Japan. We express our thanks to Prof. T. Noguchi at the College of Science of Ibaraki University, Japan (current affiliation: Faculty of Arts and Science of Kyusyu University, Japan) for his help with the TEM observations.

References

Aubert T, Soenen SJ, Wassmuth D, Cirillo M, Deun RV, Braeckmans K, Hens Z (2014) Bright and stable CdSe/CdS@SiO_2 nanoparticles suitable for long-term cell labeling. ACS Appl Mater Interfaces 6:11714–11723

Ayame T, Kobayashi Y, Nakagawa T, Gonda K, Takeda M, Ohuchi N (2011) Preparation of silica-coated AgI nanoparticles by an amine-free process and their X-ray imaging properties. J Ceram Soc Jpn 119:397–401

Bell NC, Minelli C, Tompkins J, Stevens MM, Shard AG (2012) Emerging techniques for submicrometer particle sizing applied to Stöber silica. Langmuir 28:10860–10872

Bereza-Malcolm LT, Mann G, Franks AE (2015) Environmental sensing of heavy metals through whole cell microbial biosensors: a synthetic biology approach. ACS Synth Biol. doi:10.1021/sb500286r

Betzer O, Shwartz A, Motiei M, Kazimirsky G, Gispan I, Damti E, Brodie C, Yadid G, Popovtzer R (2014) Nanoparticle-based CT imaging technique for longitudinal and quantitative stem cell tracking within the brain: application in neuropsychiatric sisorders. ACS Nano 8:9274–9285

Bitter JL, Duncan GA, Beltran-Villegas DJ, Fairbrother DH, Bevan Michael A (2013) Anomalous silica colloid stability and gel layer mediated interactions. Langmuir 29:8835–8844

Börner M, Noisser T, Reichenauer G (2013) Cross-linked monolithic xerogels based on silica nanoparticles. Chem Mater 25:3648–3653

Chou KS, Liu HL, Kao LH, Yang CM, Huang SH (2014) A quick and simple method to test silica colloids' ability toresist aggregation. Colloids Surf A 448:115–118

Cole LE, Vargo-Gogola T, Roeder RK (2014) Contrast-enhanced X-ray detection of breast microcalcifications in a murine model using targeted gold nanoparticles. ACS Nano 8:7486–7496

Geißler D, Linden S, Liermann K, Wegner KD, Charbonnière LJ, Hildebrandt N (2014) Lanthanides and quantum dots as Förster resonance energy transfer agents for diagnostics and cellular imaging. Inorg Chem 53:1824–1838

Goertz V, Gutsche A, Dingenouts N, Nirschl H (2012) Small-angle X-ray scattering study of the formation of colloidal SiO2 Stöber multiplets. J Phys Chem C 116:26938–26946

Hu Y, Shi Y, Jiang H, Huang G, Li C (2013) Scalable preparation of ultrathin silica-coated Ag nanoparticles for SERS application. ACS Appl Mater Interfaces 5:10643–10649

Jiang S, Zhuang J, Wang C, Li J, Yang W (2012) Highly efficient adsorption of DNA on Fe^{3+}-iminodiacetic acid modified silica particles. Colloids Surf A 409:143–148

Kim JM, Chang SM, Kim S, Kim KS, Kim J, Kim WS (2009) Design of SiO_2/ZrO_2 core-shell particles using the sol-gel process. Ceram Inter 35:1243–1247

Kobayashi Y, Nozawa T, Takeda M, Ohuchi N, Kasuya A (2010a) Direct silica-coating of quantum dots. J Chem Eng Jpn 43:490–493

Kobayashi Y, Nozawa T, Nakagawa T, Gonda K, Takeda M, Ohuchi N, Kasuya A (2010b) Direct coating of quantum dots with silica shell. J Sol-Gel Sci Technol 55:79–85

Kobayashi Y, Inose H, Nakagawa T, Gonda K, Takeda M, Ohuchi N, Kasuya A (2011) Control of shell thickness in silica-coating of

Au nanoparticles and their X-ray imaging properties. J Colloid Interface Sci 358:329–333
Kobayashi Y, Nozawa T, Nakagawa T, Gonda K, Takeda M, Ohuchi N (2012a) Fabrication and fluorescence properties of multilayered core-shell particles composed of quantum dot, gadolinium compound and silica. J Mater Sci 47:1852–1859
Kobayashi Y, Ayame T, Nakagawa T, Gonda K, Ohuchi N (2012b) X-ray imaging technique using colloid solution of AgI/silica/poly(ethylene glycol) nanoparticles. Mater Focus 1:127–130
Kobayashi Y, Matsudo H, Nakagawa T, Kubota Y, Gonda K, Takeda M, Ohuchi N (2013a) In-vivo fluorescence imaging technique using colloid solution of multiple quantum dots/silica/poly(-ethylene glycol) nanoparticles. J Sol-Gel Sci Technol 66:31–37
Kobayashi Y, Inose H, Nakagawa T, Kubota Y, Gonda K, Ohuchi N (2013b) X-ray imaging technique using colloid solution of Au/silica core-shell nanoparticles. J. Nanostruct Chem 3:62
Kobayashi Y, Inose H, Nagasu R, Nakagawa T, Kubota Y, Gonda K, Ohuchi N (2013c) X-ray imaging technique using colloid solution of Au/silica/poly(ethylene glycol) nanoparticles. Mater Res Innov 17:507–514
Kobayashi Y, Ayame T, Nakagawa T, Kubota Y, Gonda K, Ohuchi N (2013d) Preparation of AgI/silica/poly(ethylene glycol) nanoparticle colloid solution and X-ray imaging using it. ISRN Nanomater 2013:670402
Kobayashi Y, Nagasu R, Shibuya K, Nakagawa T, Kubota Y, Gonda K, Ohuchi N (2014) Synthesis of a colloid solution of silica-coated gold nanoparticles for X-ray imaging applications. J Nanopart Res 16:2551
Kobayashi Y, Matsudo H, Kubota Y, Nakagawa T, Gonda K, Ohuchi N (2015) Preparation of silica-coated quantum dot nanoparticle colloid solutions and their application in in vivo fluorescence imaging. J Chem Eng Jpn 48:112–117
Liang A, Liu Q, Wen G, Jiang Z (2012) The surface-plasmon-resonance effect of nanogold/silver and its analytical applications. Trends Anal Chem 37:32–47
Lismont M, Dreesen L (2012) Comparative study of Ag and Au nanoparticles biosensors based on surface plasmon resonance phenomenon. Mater Sci Eng C 32:1437–1442
Lusic H, Grinstaff MW (2013) X-ray-computed tomography contrast agents. Chem Rev 113:1641–1666
Ma Y, Li Y, Zhong X (2014) Silica coating of luminescent quantum dots prepared in aqueous media for cellular labeling. Mater Res Bull 60:543–551
Mondragon R, Julia JE, Barba A, Jarque JC (2012) Characterization of silica-water nanofluids dispersed with an ultrasound probe: a study of their physical properties and stability. Powder Technol 224:138–146
Neville F, Zin AM, Jameson GJ, Wanless EJ (2012) Preparation and characterization of colloidal silica particles under mild conditions. J Chem Educ 89:940–942
Ozawa T, Yoshimura H, Kim SB (2013) Advances in fluorescence and bioluminescence imaging. Anal Chem 85:590–609
Sapsford KE, Algar WR, Berti L, Gemmill KB, Casey BJ, Oh E, Stewart MH, Medintz IL (2013) Functionalizing nanoparticles with biological molecules: developing chemistries that facilitate nanotechnology. Chem Rev 113:1904–2074
Scoditti E, Massaro M, Montinari MR (2013) Endothelial safety of radiological contrast media: why being concerned. Vasc Pharmacol 58:48–53
Tassali N, Kotera N, Boutin C, Léonce E, Boulard Y, Rousseau B, Dubost E, Taran F, Brotin T, Dutasta JP, Berthault P (2014) Smart detection of toxic metal ions, Pb^{2+} and Cd^{2+}, using a ^{129}Xe NMR-based densor. Anal Chem 86:1783–1788
Ujihara M, Imae T (2013) Versatile one-pot synthesis of confeito-like Au nanoparticles and their surface-enhanced Raman scattering effect. Colloids Surf A 436:380–385
Wang S, Li C, Yang P, Ando M, Murase N (2012) Silica encapsulation of highly luminescent hydrophobic quantum dots by two-step microemulsion method. Colloids Surf A 395:24–31
Wendel FM, Eversloh CL, Machek EJ, Duirk SE, Plewa MJ, Richardson SD, Ternes TA (2014) Transformation of Iopamidol during chlorination. Environ Sci Technol 48:12689–12697
Yang Y, Mathieu JM, Chattopadhyay S, Miller JT, Wu T, Shibata T, Guo W, Alvarez PJJ (2012) Defense mechanisms of pseudomonas aeruginosa PAO1 against quantum dots and their released heavy metals. ACS Nano 6:6091–6098
Young M, Santra S (2014) Copper (Cu)-ailica nanocomposite containing valence-engineered Cu: a new strategy for improving the antimicrobial efficacy of Cu biocides. J Agric Food Chem 62:6043–6052
Zeng Q, Zhang Y, Ji W, Ye W, Jiang Y, Song J (2014) Inhibitation of cellular toxicity of gold nanoparticles by surface encapsulation of silica shell for hepatocarcinoma cell application. ACS Appl Mater Interfaces 6:19327–19335
Zhang C, Uchikoshi T, Kitabatake T, Sakka Y, Hirosaki N (2013) Surface modification of Ca-α-SiAlON: Eu^{2+} phosphor particles by SiO_2 coating and fabrication of its deposit by electrophoretic deposition (EPD) process. Appl Surf Sci 280:229–234